© 2020. Published by The Company of Biologists Ltd | Journal of Experimental Biology (2020) 223, jeb196535. doi:10.1242/jeb.196535

RESEARCH ARTICLE

Mind the gap: natural cleft palates reduce biting performance in bats

Abigail A. Curtis[1,*], Jessica H. Arbour[1] and Sharlene E. Santana[1,2]

ABSTRACT

Novel morphological traits pose interesting evolutionary paradoxes when they become widespread in a lineage while being deleterious in others. Cleft palate is a rare congenital condition in mammals in which the incisor-bearing premaxilla bones of the upper jaw develop abnormally. However, ∼50% of bat species have natural, non-pathological cleft palates. We used the family Vespertilionidae as a model and linear and geometric morphometrics within a phylogenetic framework to (1) explore evolutionary patterns in cleft morphology, and (2) test whether cleft morphological variation is correlated with skull shape in bats. We also used finite element (FE) analyses to experimentally test how presence of a cleft palate impacts skull performance during biting in a species with extreme cleft morphology (hoary bat, *Lasiurus cinereus*). We constructed and compared the performance of two FE models: one based on the hoary bat's natural skull morphology, and another with a digitally filled cleft simulating a complete premaxilla. Results showed that cleft length and width are correlated with skull shape in Vespertilionidae, with narrower, shallower clefts seen in more gracile skulls and broader, deeper clefts in more robust skulls. FE analysis showed that the model with a natural cleft produced lower bite forces, and had higher stress and strain than the model with a filled cleft. In the rostrum, safety factors were 1.59–2.20 times higher in the model with a filled cleft than in the natural model. Our results demonstrate that cleft palates in bats reduce biting performance, and evolution of skull robusticity may compensate for this reduction in performance.

KEY WORDS: Biting, Cranial morphology, Finite element analysis, Geometric morphometrics, Bats, Vespertilionidae

INTRODUCTION

The evolution of novel morphological traits can have great impacts on organismal performance during behaviors critical to survival (e.g. feeding), which in turn is expected to determine the evolutionary prevalence of such morphologies (Erwin, 2015). Novel traits are especially puzzling from an evolutionary perspective when they become widespread within a lineage while being deleterious in other lineages. In mammals, cleft palate is a rare congenital condition that results from abnormal development of the paired premaxilla bones, which bear the upper incisors in the anterior region of the upper jaw (Dixon et al., 2011). Cleft palate is best known in humans, and has been documented in other primates (Krief et al., 2015), as well as some domesticated animals such as dogs (Paradas-Lara et al., 2014), cows (Myers et al., 1996) and rodents (Satokata and Maas, 1994), although it appears to be extremely rare in wild individuals (Krief et al., 2015). In non-human species, cleft palate is often associated with additional congenital defects (Dixon et al., 2011). However, naturally occurring orofacial clefts have evolved independently at least eight times in bats (Order Chiroptera, >1400 species), and are present in >50% of all extant species (Giannini and Simmons, 2007; Hutcheon and Kirsch, 2006; Orr et al., 2016; Simmons and Geisler, 1998). Bat orofacial clefts may be medial or paramedial with the intervening space filled with fibrous tissue that creates a flexible, complete-looking, dental arch (Giannini and Simmons, 2007; Hutcheon and Kirsch, 2006; Orr et al., 2016; Simmons and Geisler, 1998). Building a better understanding of cleft evolution, development and morphological variation in bats may therefore contribute to our understanding of congenital cleft palates in other taxa (Diogo et al., 2015, 2017; Orr et al., 2016).

The mechanisms that led to the repeated evolution of orofacial clefts and their prevalence among bats are poorly understood. Several authors have posed adaptive hypotheses to explain the evolution of orofacial clefts in bats; clefts may allow greater mobility or increased gape at the tip of the rostrum for grooming, prey capture or shaping the echolocation call beam when bats emit sound via the mouth or nostrils (Giannini and Simmons, 2007; Hutcheon and Kirsch, 2006; Orr et al., 2016; Simmons and Geisler, 1998). Reduction of the premaxilla bone could also aid in reducing skull mass for flight efficiency (Giannini and Simmons, 2007; Hutcheon and Kirsch, 2006; Orr et al., 2016; Simmons and Geisler, 1998). However, there is no current consensus on the function of cleft palates in bats, and alternatives to these adaptive hypotheses have yet to be investigated. For example, clefts may be a consequential trade-off with a different trait that increases overall fitness of bats, or may represent a case of an ecomorphological mismatch owing to genetic or developmental constraints (Alberch, 1989; Galis, 1999).

A question that naturally arises with respect to the recurrent evolution of orofacial clefts in bats is how the loss of a rigid bony connection between the canines impacts skull performance during prey capture and feeding, both of which are imperative to fitness in bats. Bats use their canine teeth to capture, kill, transport and manipulate prey (Freeman, 1992). The presence of a cleft between the canines likely increases the level of bone stress and deformation that the rostrum experiences during biting owing to the loss of structural support between the canines. The presence of a cleft may also reduce a bat's ability to transfer muscle force from the jaw-closing muscles into bite force at the biting point as a consequence of energy loss via deformation of the rostrum. This, in turn, may limit the hardness of foods that a bat with a cleft palate can successfully capture and eat, or could result in the evolution of compensatory morphological changes in the skull, jaw musculature and/or specialized biting behaviors. To date, it is unknown how the presence of a cleft impacts the biomechanical performance of bat

[1]Department of Biology, University of Washington, Seattle, WA 98195-1800, USA. [2]Burke Museum of Natural History and Culture, University of Washington, Seattle, WA 98195-1800, USA.

*Author for correspondence (abigailacurtis@gmail.com)

A.A.C., 0000-0002-9774-2814

Received 16 November 2018; Accepted 12 December 2019

Journal of Experimental Biology (2020) 223, jeb196535. doi:10.1242/jeb.196535

skulls during prey capture and feeding, and how cleft size and shape vary in relation to overall skull shape in bats.

In this study, we first use geometric morphometric techniques within a phylogenetic framework to explore evolutionary patterns in cleft morphology and test whether variation in cleft morphology is correlated with skull shape in bats. We use the family Vespertilionidae as a model because it is the largest family of bats (~400 animalivorous species; Simmons, 2005), and all species in this family have a midline cleft with the maxillary branch of the premaxilla solidly fused to the maxilla. Within Vespertilionidae, cleft morphology varies from narrow, anteriorly restricted clefts (e.g. *Myotis*) to broad, deep clefts (e.g. *Lasiurus*). Mechanical properties of prey also vary among species in this family, ranging from soft prey, such as moths, to hard prey, such as beetles and even other vertebrates (Freeman, 1981; Freeman and Lemen, 2007). If cleft morphology (e.g. relative size, shape and position) limits the performance of the skull during feeding, then we expect to find a correlation between cleft morphology and other aspects of skull shape that are predictive of bite performance, such as rostral dimensions, the size of jaw adductor muscle attachment areas, and cranial height (Dumont et al., 2012; Freeman, 1979, 1981; Santana and Cheung, 2016; Santana et al., 2012).

Second, we empirically test the hypothesis that orofacial clefts reduce skull bite performance. To do so, we compare the outcomes of analyses on two finite element (FE) models of the skull of a hoary bat, *Lasiurus cinereus*, which simulate prey capture and chewing behaviors. The first model is based on the natural skull morphology of the hoary bat, which has a broad, deep midline cleft, and the second model has a digitally filled cleft to mimic a complete dental arch. Finite element analysis is an engineering method that has been successfully used to test how differences in form and material properties affect the mechanical performance of geometrically complex biological structures (Bohmann et al., 2011; Dumont et al., 2005; Slater et al., 2009; Tseng and Wang, 2011; Wroe et al., 2005).

We predict several key differences in biting performance between the model with a cleft versus the model with a filled cleft (Fig. 1). First, we predict that a skull with a cleft palate will produce lower bite force than a skull with a complete palate. This is because the anterior region of the rostrum is likely less rigid in the skull with a cleft palate owing to loss of the bony connection between the left and right canines, which would cause muscle force to be lost as strain energy (energy loss owing to deformation). Additionally, we predict that bending of the rostrum and palate during bilateral biting at the canine teeth (biting with both canines) is greater in the skull with a cleft palate, thus the model with a cleft palate should show greater concentrations of stress in the maxillary and palatal regions than the model with a filled cleft. We also expect lower resistance to torsional (twisting) stress during unilateral biting at the canine tooth (biting with one canine) in the model with a cleft palate, and higher and more concentrated regions of stress in the maxillary region on the biting side in the model with a cleft versus the model with a complete palate.

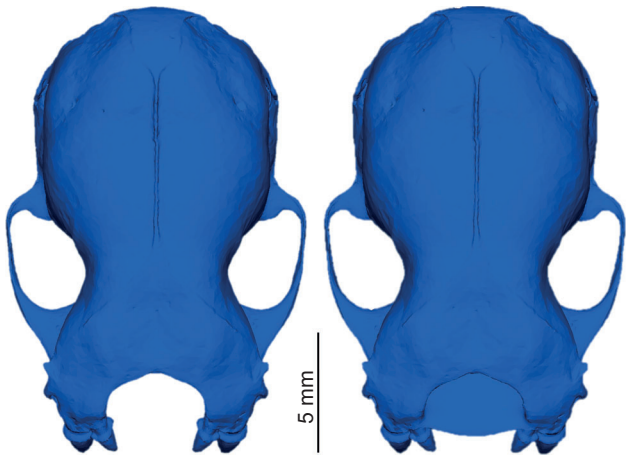

Fig. 1. Finite element models used in this study. Predictions for mechanical advantage (MA), stress and strain energy are shown below each model.

MATERIALS AND METHODS

Orofacial cleft morphology and skull shape

To accurately quantify cleft and cranial morphology for comparative analyses, we µCT scanned the crania of 68 specimens representing 34 species and 24 genera of vespertilionid bats (approximately 50% generic coverage, 1–4 individuals per species; Table S1). We scanned crania at the American Museum of Natural History, New York, NY, USA, using a GE Phoenix V|tome|x µCT scanner (General Electric, USA) with a 240 kV X-ray tube, and a Skyscan 1172 µCT scanner (Bruker µCT, Belgium) at the University of Washington, Seattle, WA, USA. Scan resolution (voxel size) depended on skull size and ranged from 8.09 to 40.90 µm (Table S1). We generated tiff or BMP formatted image stacks from raw µCT data using Phoenix Datos|x (General Electric, USA) or NRecon (Bruker µCT). We manually segmented skulls from µCT data using Mimics v. 20 (Materialise, NV, Leuven, Belgium), and exported skull 3D surface meshes as binary .STL files. We further edited these meshes using Geomagic Studio 2014 (Geomagic Inc., Research Triangle Park, NC, USA) to remove scan artifacts and reduce mesh size prior to landmark placement for geometric morphometric analyses. A recent study, which included a sample of 435 bat skulls that were µCT scanned using a similar range of voxel sizes and segmentation protocol, showed a <2% difference between linear measurements taken from physical skulls and their digital representations (Shi et al., 2018). Therefore, we expect that our µCT dataset accurately captures the cranial morphology of the species in our sample.

To test for a relationship between cleft palate shape and size and skull characteristics, we first determined the position and anteroposterior length of the cleft in relation to the dentition of each bat by examining skulls in ventral view with the plane of the palate oriented perpendicularly to the line of sight. Then, a single observer (J.H.A.) placed each species into one of three groups, in which the position of the posteriormost point of the cleft between the teeth either (1) does not reach the alveolus of the first premolar, (2) reaches past the alveolus first premolar but not past the anterior margin of the first molar alveolus or (3) reaches past the anterior of the first molar alveolus (Fig. S1; Fig. 2). Based on these groups, we reconstructed the evolutionary history of cleft palate position relative to the dental arcade using stochastic character mapping with asymmetric transition rates, and a subtree taken from a recent phylogeny of bats (Shi and Rabosky, 2015). We used the R function make.simmap in the package phytools (Bollback, 2006; Huelsenbeck et al., 2003; Revell, 2012) to conduct these analyses.

To quantify cleft shape variation and its relation to skull shape in our sample, we conducted phylogenetically informed geometric

Journal of Experimental Biology (2020) 223, jeb196535. doi:10.1242/jeb.196535

morphometric analyses. A single observer (J.H.A.) used Checkpoint v. 2017 (Stratovan, Davis, CA, USA) to place a bilaterally symmetrical series of 36 landmarks and five semi-landmark curves on each cranium, and three landmarks and two semi-landmark curves outlining the cleft (Fig. S2, landmark descriptions provided in Table S2). We estimated a small percentage of missing landmarks (owing to specimen damage, largely the zygomatic arches and auditory bullae) by first exploiting bilateral symmetry via reflected relabeling, and then Bayesian principal components analysis (PCA) for all remaining missing landmarks (Arbour and Brown, 2014; Brown et al., 2012; Gunz et al., 2009; Oba et al., 2003). We used functions within the R package geomorph to perform generalized Procrustes superimpositions and other geometric morphometric analyses on the cleft palate and cranial landmark datasets individually. We averaged landmark coordinates across individuals within each species and across bilaterally symmetrical landmarks (function mshape; Adams and Otárola-Castillo, 2013; package geomorph, https://cran.r-project.org/web/packages/geomorph/index.html), and tested for phylogenetic signal in each of the cleft palate and cranial landmark datasets (function physignal; Blomberg et al., 2003; Adams, 2014). We summarized variation in cranial and cleft palate shape using phylogenetic PCA (pPCA) (Revell, 2009), and selected critical axes through parallel analysis (Horn, 1965; Peres-Neto et al., 2005).

To investigate whether cleft palate shape or relative size is associated with cranial shape, we first ran a two-block partial least squares (PLS) test on the two landmark datasets (Rohlf and Corti, 2000). We implemented a phylogenetic correction to the PLS using the R function phylo.integration (Adams and Felice, 2014). We additionally contrasted the relative width of the cleft and relative length of the cleft, respectively, with cranial shape using procD.pgls. Preliminary observations suggested that relative size of the cleft, in addition to shape of the cleft perimeter, could be correlated with skull shape. We determined the relative length of the cleft palate by taking the ratio of the distance between the anteriormost landmark and posteriormost landmark along the midline of the palate to bizygomatic width. We quantified the relative width of the cleft palate by taking the ratio of the horizontal distance across the widest point of the cleft to the greatest skull length (distance from the anteriormost point of the premaxilla to the intersection of the sagittal and lamboidal crests).

Finite element methods

We constructed two FE models based on the dry skull of an adult *Lasiurus cinereus* (University of Washington Burke Museum; UWBM 63244). This species was selected because it has an extreme cleft shape among vespertilionids in our sample (see Results). We µCT scanned the specimen at a 12.01 µm resolution using a Skyscan 1172 µCT scanner at the University of Washington, Seattle. Following the protocol of Dumont et al. (2005), we segmented the skull and dentary from µCT slices in Mimics. We used Geomagic Studio to edit skull and dentary meshes in preparation for FE analysis. Skull structures with complicated geometries and FE meshes with large numbers of elements often result in computational errors or can be too computationally complex for FE software to handle (Dumont et al., 2005). Therefore, we removed structures such as the turbinal bones within the nasal chamber, reduced the number of foramina in the cribriform plate by approximately 50%, filled the inner ear and largely removed trabecular bone. Using Mimics 3-Matic 12.0, we then generated a solid, four-noded tetrahedral FE mesh of the cranium with a geometric error tolerance of 0.01201 mm (the voxel size for the original µCT scan) to minimize model distortion. This first model approximates the natural cleft morphology of *L. cinereus* (Fig. 1, natural cleft). To ensure that differences between models were solely due to differences in cleft morphology, we modified the first model in Geomagic Studio by artificially filling the natural cleft to approximate the shape and dimensions of a complete premaxilla. Then, we used 3-Matic to generate a second FE mesh (Fig. 1, filled cleft). We exported FE meshes as Nastran files for subsequent analyses. The model with a natural cleft was composed of 581,442 elements with a surface area of 1239.39 mm^2 and a volume of 139.457 mm^3, and the model with a filled cleft was composed of 583,128 elements with a surface area of 1256.16 mm^2 and a volume of 141.273 mm^3.

Using Strand7 v. R2.4.5 (Strand7 Pty Ltd, Sydney, Australia), we assigned both skull models isotropic material properties for mammalian cortical bone (Young's modulus: $E=2.512\times10^4$ MPa, Poisson's ratio: $\nu=0.3$; Erickson et al., 2002; Dumont et al., 2009). For all feeding simulations, we constrained the temporomandibular joint movement in the *x*-, *y*- and *z*-axes on the left side and the *y*- and *z*-axes on the right side in order to not over-constrain the models (Dumont et al., 2005; Santana and Dumont, 2011). These two nodes represented contact between the cranium and the dentary. We constrained the teeth in the *z*-axis, which was perpendicular to the hard palate, and simulated four biting behaviors that insectivorous bats commonly use during prey capture and mastication. Insectivorous bats use their canine teeth to capture, kill and transport prey (Freeman, 1992, 1998), and they may bite into prey with both (bilateral) or a single (unilateral) canine tooth during these behaviors. To model a bilateral canine bite, we constrained nodes at the tips of both canines. To model a unilateral canine bite, we constrained a node at the tip of the left canine. Insectivorous bats use their molars to break up an insect's exoskeleton prior to swallowing, and they may engage one or both of their molars during chewing depending on the size of the prey item (Freeman, 1998). To simulate bilateral chewing at the molars, we constrained nodes at the tips of both M1 paraconids. To simulate unilateral chewing at the molars, we constrained a single node at the tip of the left M1 paraconid.

We used Boneload v.6 (Dumont et al., 2009; Grosse et al., 2007) to distribute muscle forces across the origins of the major jaw adductor muscles (m. temporalis, m. masseter, m. pterygoideus medialis) during biting behavior simulations. Boneload models the effects of wrapping of jaw adductor muscles and their forces around the curved surfaces of the cranium. This eliminates artifacts owing to point loading, and results in a more accurate representation of stress distributions across muscle attachment sites in FE models (Grosse et al., 2007). We estimated the relative contributions of each jaw adductor to bite force based on their masses, which have been reported for *L. cinereus* by Freeman and Lemen (2010). Because their study measured the combined masses of the temporalis and pterygoideus muscles, we modeled the origins of these two muscles as a single area on each side of the cranium. We do not expect our stress/strain pattern results to be impacted significantly by this because the pterygoideus muscle contributes <10% of the total jaw adductor mass, on average, in other bats (Herrel et al., 2008; Santana et al., 2010). We assumed that all muscles were contracting maximally and simultaneously based on previous electromyography studies in other bats and mammals (De Gueldre and De Vree, 1988; Hylander et al., 2004).

Boneload requires each muscle force vector to be directed toward a single point representing the muscle's insertion site on the mandible. We positioned the dentary at an intermediate gape angle (30 deg; Davis et al., 2010; Santana et al., 2010, 2012) and directed

Journal of Experimental Biology (2020) 223, jeb196535. doi:10.1242/jeb.196535

muscle force vectors from their origins toward the centroids of their respective insertion areas on the dentary. We obtained these centroids by running the 'Area Centroids' algorithm in Boneload (Davis et al., 2010; Grosse et al., 2007) on binary STL files of insertion areas, which we defined and exported from Geomagic Studio. We used the Gradient Traction method in Boneload (Davis et al., 2010) to apply muscle forces across attachment sites for the temporalis, pterygoideus and masseter. We loaded both FE models using identical muscle attachment areas and centroids. All feeding behavior simulations were modeled using Linear Static Analysis in Strand 7 (Dumont et al., 2005).

Size and shape differences between FE models can impact predicted bite force, stress and strain magnitudes (Dumont et al., 2009). Because we are interested in how differences in cleft shape affect mechanical performance under different loading conditions, we scaled our models to the same size based on the methods in Dumont et al. (2009). Our null expectation was no difference in relative bite forces, stress and strain distribution or magnitude between models, which would suggest no difference in performance. Thus, any differences in these variables should be strictly due to shape differences (i.e. presence versus absence of a cleft).

In order to compare bite force and von Mises stress magnitudes and distributions among models, we scaled the ratio of muscle force to model surface area to be equivalent between both models (Dumont et al., 2009; Slater et al., 2009). We calibrated muscle forces acting on the natural skull model to 10.4 N, to produce a bilateral canine bite force of 6.8 N in the dorso-ventral direction, based on bite force measured from a live *L. cinereus* by Freeman and Lemen (2010). Then, we scaled the muscle forces acting on the model with a filled cleft to 10.54 N to produce the same muscle force:surface area ratio as the natural model. To compare the ability to transfer muscle force into bite force, we computed the mechanical advantage (bite force produced:muscle force ratio) from each feeding simulation, as our two models differed in surface area (Dumont et al., 2009). We used contour plots to visualize von Mises stress distributions across models, compared histograms of von Mises stress across elements forming the dorsal portion of the rostrum and palate, and computed mean and maximum stress for the rostrum and palate in the regions shown in Fig. S3 for both models across the four feeding behavior simulations. To gain a better quantitative understanding of the degree to which a cleft impacts skull strength, we also calculated safety factors for each model (Gilbert et al., 2016) by dividing the stress value at which bone fails (140 MPa; Nordin and Frankel, 2001; Dumont et al., 2005) by the maximum stress value from each model/simulation. A safety factor closer to 1 indicates that a structure is near its failure point under the applied load, whereas a higher safety factor indicates that a structure is more resistant to breaking under the applied load.

To compare strain energy between models, we scaled the muscle forces acting on the model with a filled cleft to 10.42 N, such that the ratio of muscle force to the model's volume$^{1/6}$ was equivalent to that for the model with a natural cleft (based on Dumont et al., 2009; Slater et al., 2009). We then obtained mean and maximum strain values from the rostrum and palate, respectively, for both models from all four feeding behavior simulations.

RESULTS

Morphological diversity of cleft palates in vesper bats

The majority of species examined had cleft palates that extended as far posteriorly as the pre-molars but not to the molars (Fig. 2). Evolutionary shifts were observed only from this most common character state for clefts in vespertilionids to clefts that did not reach the premolars, or clefts that reached past the first molar (Fig. 2). Both the cranial and cleft palate landmark datasets showed significant phylogenetic signal (K=1.06 and 0.81, respectively, both P=0.001). pPCA of cleft shape in 34 species revealed two critical axes describing 77.6% of variation in cleft shape (Fig. 3). Shape variation on pPC1 ranged from broad clefts (−) to narrow clefts (+). Comparatively, pPC2 described a gradient from smoothly tapered (+) to rounded and blunt clefts (−) (Fig. 3). Both *Lasiurus* species in our sample exhibited extreme morphologies across both axes, with the broadest and most tapered clefts among the species examined (Fig. 3).

Overall cleft shape was not significantly correlated with cranial shape after phylogenetic correction (PLS r=0.547, P=0.120). However, both relative length and width of the cleft were correlated with cranial shape (width ratio: PLS r=0.402, P=0.001; length ratio: PLS r=0.461, P=0.001). Wider and deeper clefts were both associated with broader, more robust skull shapes (taller and stouter) with proportionally shorter rostra (Fig. 4).

Mechanical effects of cleft palate

During bilateral canine bite simulations, contour plots of von Mises stress showed similar patterns across both models of *L. cinereus*' skull, with stress concentrations on the dorsolateral surfaces of the rostrum, as well as along the dorsomedial margin of the external narial aperture. Both of these patterns reflect dorsal bending of the rostrum (Fig. 5). On the palate, stress was most concentrated in the posterolateral region, with moderate concentrations along the alveolar borders of the molars (Fig. 5). Overall, the model with a filled cleft performed better than the model with a natural cleft; it showed a higher bite force:muscle force ratio (mechanical advantage), lower mean and maximum von Mises stress and strain energy in the rostrum, and more even distribution of stress across the dorsal surface of the rostrum and on the palate (Fig. 5, Table 1, Fig. S4). Most of the filled region in the filled cleft model was under relatively low stress, but stress did reach the filled region (Fig. 5). The mechanical advantage for the model with a filled cleft was 3% higher than in the model with a natural cleft. Maximum stress in the rostrum of the model with a filled cleft was 58% of that measured in the natural model, while maximum strain in the rostrum was 66% of that in the natural model. However, maximum von Mises stress and strain energy in the palate were lower in the model with a natural cleft, albeit similar in magnitude to maximum von Mises stress and strain energy measured in the palate of the filled model (2% and 3% higher in the filled model, respectively; Fig. 5, Table 1). Average von Mises stress and strain energy in the palate were lower in the model with a filled cleft, likely driven by the low stress and strain in the filled region (Fig. 5, Table 1). Safety factors for the natural and filled models during bilateral canine biting were 2.20 and 3.77 for the rostrum, and 1.83 and 1.79 for the palate, respectively.

During simulation of unilateral canine biting, von Mises stress was more concentrated on the biting side of the skull, indicating torsional (twisting) stress (Fig. 5). The model with a filled cleft performed better than the model with a natural cleft and showed greater mechanical advantage, lower mean and maximum von Mises stress and strain energy in both the rostrum and palate, and a more even distribution of stress across the rostrum and palate in contour plots (Fig. 5, Table 1, Fig. S4). Again, stress in the palate of the model with a filled cleft reached the filled region, resulting in more even dissipation of stress across the palate (Fig. 5). Mechanical advantage was 3% higher in the model with a filled cleft than in the model with a natural cleft (Table 1). Maximum von Mises stress and

Journal of Experimental Biology (2020) 223, jeb196535. doi:10.1242/jeb.196535

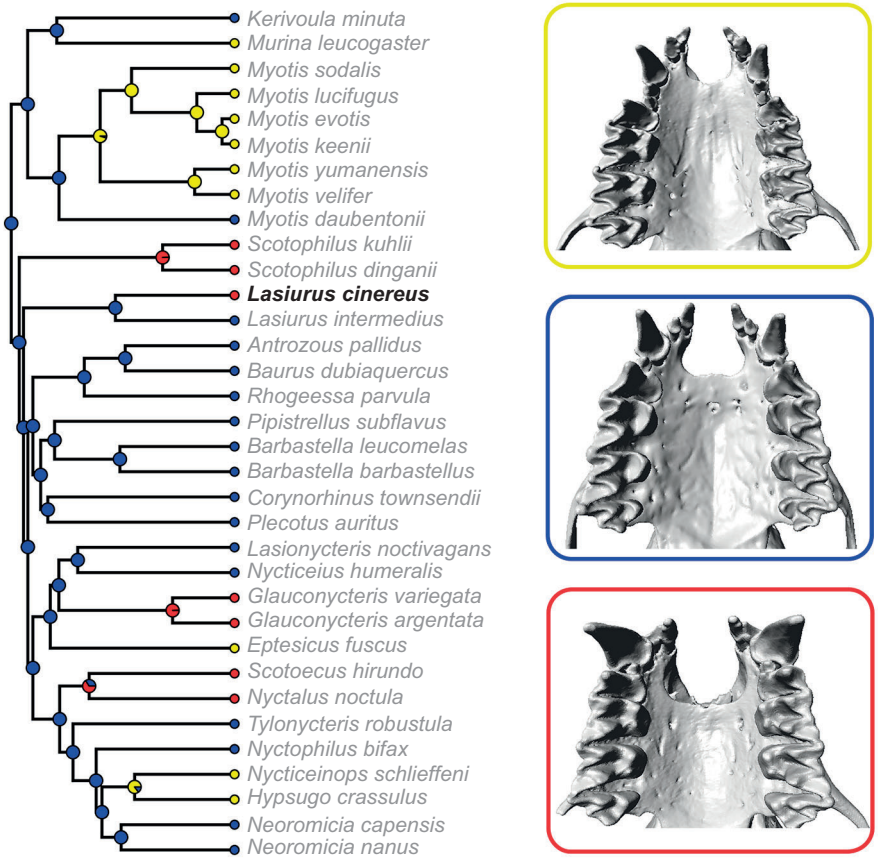

Fig. 2. Ancestral state reconstructions for position of the posterior margin of the cleft relative to the dentition in Vespertilionidae. Yellow: cleft does not extend posteriorly past the premolars; blue: cleft extends posteriorly past the premolars; red: cleft extends posteriorly past the first molar. Crania illustrating these morphologies are shown to the right of the phylogeny.

strain energy in the rostrum of the filled model were 63% and 38%, respectively, of that measured in the rostrum of the natural model. Despite the fact that the model with a filled cleft showed lower maximum von Mises stress and strain energy than the model with a natural cleft, these were very similar in magnitude (>99% and 96%, respectively, of that measured in the palate of the natural model;

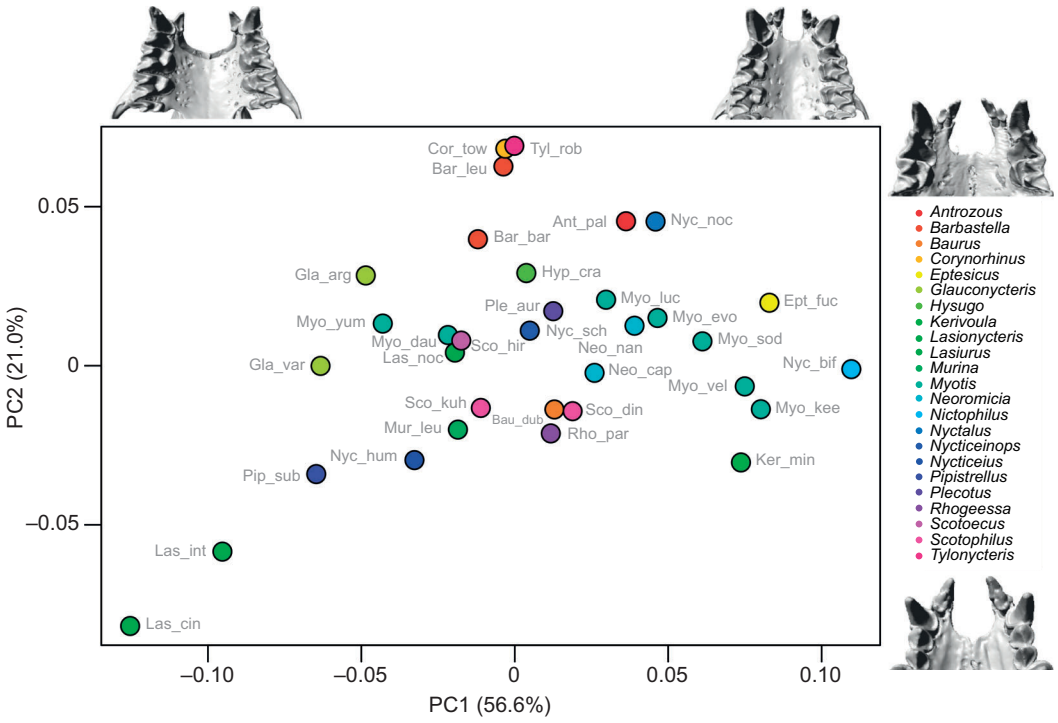

Fig. 3. Phylogenetic PCA of species means for cleft shape based on landmark and semi-landmark configurations. Extremes for cleft morphologies are shown along each axis. Points are colored based on genus, and species abbreviations can be found in Table S1.

Journal of Experimental Biology (2020) 223, jeb196535. doi:10.1242/jeb.196535

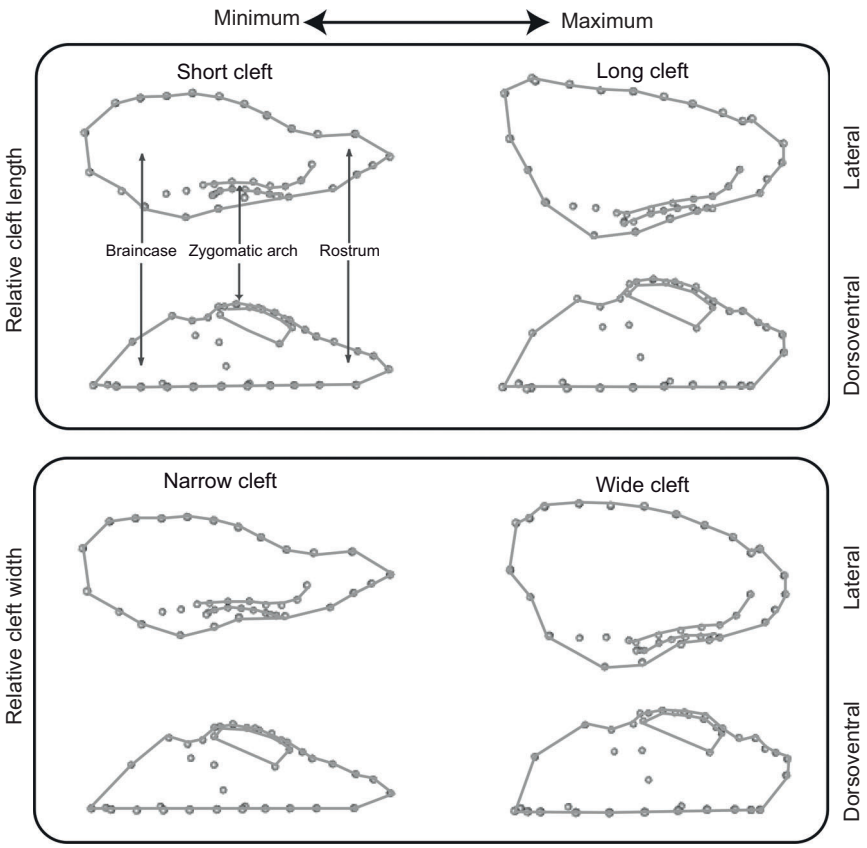

Fig. 4. Skull shape variation associated with relative cleft length (top) and relative cleft width (bottom) based on a partial least squares analysis of bilaterally averaged 3D landmark coordinates. Landmarks (dots) show the fitted values of cranial shape corresponding to the maximum and minimum relative cleft length and width.

Fig. 5, Table 1). Safety factors for the natural and filled models during unilateral canine biting were 1.85 and 2.95 for the rostrum, and 1.64 and 1.65 for the palate, respectively.

A simulation of bilateral molar biting as a proxy for chewing showed patterns of von Mises stress similar to those from our simulations of bilateral canine biting across the rostrum and palate in both models (Fig. 6). However, concentrations of stress on the dorsal surface of the rostrum were more restricted in size compared with those in simulations of canine bites. During bilateral molar biting, the model with a filled cleft performed better than the model with a natural cleft with greater mechanical advantage, lower mean and maximum von Mises stress and strain energy in the rostrum and

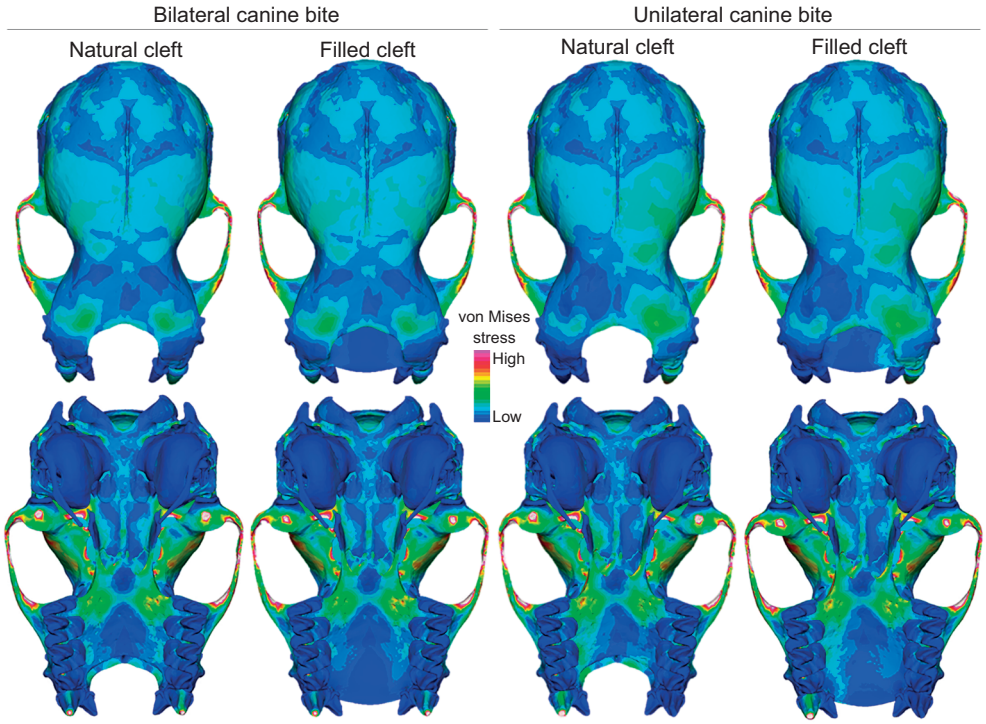

Fig. 5. Contour plots showing von Mises stress distribution across natural and filled cleft models during bilateral and unilateral canine biting. Range of von Mises stress shown on skulls is 0–9 MPa.

Journal of Experimental Biology (2020) 223, jeb196535. doi:10.1242/jeb.196535

Table 1. Summary of mean and maximum von Mises stress, mean and maximum strain energy, and mechanical advantage (MA) for the four biting simulations in the finite element model with a natural cleft and a filled cleft

Behavior	Region	Model	Stress (MPa) mean, max.	Strain (J mm^{-3}) mean, max.	MA
BC bite	Rostrum	Natural	14.22, 63.50	5.00×10^{-6}, 8.39×10^{-5}	0.065
		Filled	**13.15**, **37.14**	**3.75×10^{-6}**, **2.36×10^{-5}**	**0.067**
	Palate	Natural	21.96, **76.55**	1.28×10^{-5}, **1.11×10^{-4}**	
		Filled	**15.88**, 78.19	**8.48×10^{-6}**, 1.14×10^{-4}	
UC bite	Rostrum	Natural	15.79, 75.62	6.41×10^{-6}, 1.08×10^{-4}	0.065
		Filled	**14.71**, **47.47**	**5.14×10^{-6}**, **4.13×10^{-5}**	**0.067**
	Palate	Natural	23.35, 85.24	1.40×10^{-5}, 1.28×10^{-4}	
		Filled	**17.70**, **85.10**	**9.32×10^{-6}**, **1.23×10^{-4}**	
BM bite	Rostrum	Natural	11.65, 64.34	3.77×10^{-6}, 8.05×10^{-5}	0.084
		Filled	**10.22**, **29.16**	**2.41×10^{-6}**, **1.44×10^{-5}**	**0.086**
	Palate	Natural	21.57, 78.14	1.26×10^{-5}, 1.13×10^{-4}	
		Filled	**15.64**, **76.66**	**8.35×10^{-6}**, **1.09×10^{-4}**	
UM bite	Rostrum	Natural	12.71, 72.96	4.35×10^{-6}, 1.05×10^{-4}	0.083
		Filled	**11.46**, **34.26**	**3.10×10^{-6}**, **2.09×10^{-5}**	**0.086**
	Palate	Natural	22.34, **82.56**	1.31×10^{-5}, 1.21×10^{-4}	
		Filled	**16.64**, 83.69	**8.78×10^{-6}**, **1.20×10^{-4}**	

BC, bilateral canine; UC, unilateral canine; BM, bilateral molar; UM, unilateral molar. Bold indicates the lower stress and strain, and highest MA in each simulation.

palate, and more even dissipation of stress across the rostrum and palate in contour plots (Fig. 6, Table 1, Fig. S4). The mechanical advantage was 2% higher in the model with a filled cleft. Maximum von Mises stress and strain energy in the rostrum of the filled model were 45% and 18%, respectively, of that in the natural model. In the palate, von Mises stress and strain energy were slightly lower in the filled model (98% and 96%, respectively, of that in the natural model). Safety factors for the natural and filled models during bilateral molar biting were 2.18 and 4.80 for the rostrum, and 1.79 and 1.83 for the palate, respectively.

Patterns of von Mises stress across the skull during simulation of unilateral molar biting were similar to those of bilateral molar biting, but more concentrated on the biting side. Again, the model with a filled cleft performed better than the model with a natural cleft and produced greater mechanical advantage, lower mean von Mises stress and mean strain energy in the rostrum and palate, with more even dissipation of stress across both regions (Fig. 6, Table 1, Fig. S4). The mechanical advantage in the filled model was 4% higher than in the natural model. Maximum stress in the palate was 1% higher in the model with a filled cleft, and strain was >99% of that measured in the model with a natural cleft. Safety factors for the natural and filled models during unilateral molar biting were 1.92 and 4.09 for the rostrum, and 1.70 and 1.67 for the palate, respectively.

DISCUSSION

Using geometric morphometrics and FE methods, we were able to characterize evolutionary patterns in orofacial cleft morphology in the largest family of bats, Vespertilionidae, and show that the presence of a cleft reduces biting performance in one species. However, evolutionary ancestry appears to explain a significant portion of orofacial cleft diversity in Vespertilionidae, as evidenced

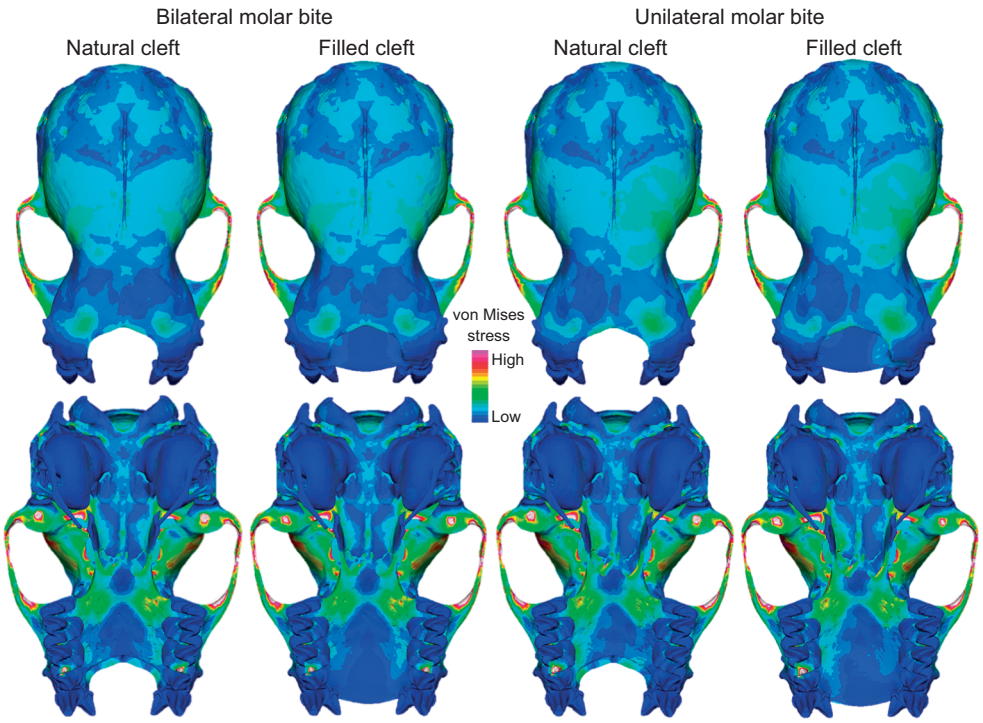

Fig. 6. Contour plots showing von Mises stress distribution across natural and filled cleft models during bilateral and unilateral molar biting. Range of von Mises stress shown on skulls is 0–9 MPa.

by strong phylogenetic signal in 3D landmark data. This indicates that cleft evolution may be, at least partially, constrained by intrinsic factors linked to common ancestry and without a clear adaptive value within the context of feeding function in vesper bats (Alberch, 1989; Diogo, 2017; Galis, 1999).

After taking phylogenetic autocorrelation into account, we found that the shape of clefts did not vary with 3D skull shape, but cleft mediolateral width and anteroposterior length were correlated with skull shape in vespertilionid bats. Our geometric morphometric analyses indicated that the shape of the cleft outline can be similar between taxa with proportionally larger or proportionally smaller clefts, which likely explains the lack of relationship between cleft outline shape and skull shape. However, when relative width and depth of the cleft are compared, mediolaterally broader, anteroposteriorly deeper clefts are associated with more robust cranial traits (broader and taller skulls with foreshortened rostra), whereas narrower, shallower clefts are correlated with a more gracile cranium shape (narrower and shorter skulls with more elongate rostra). This suggests that cleft morphology evolved in tandem with feeding function demands on the cranium. For example, given that a cleft appears to result in a weaker skull (below), it is possible that broader, deeper clefts require greater structural compensation from the rest of the cranium, resulting in correlated evolution of large clefts and cranial robusticity. Jaw muscle morphology and function could also evolve to compensate for potential detrimental effects of clefts on biting performance. Thus, future work that incorporates quantitative comparisons of jaw muscular anatomy and physiology (e.g. Herrel et al., 2008; Santana, 2018) could greatly improve our understanding of how hard and soft tissues interact and impact feeding performance in species with cleft palates.

Our results also demonstrate that clefts in vespertilionid bats most commonly extend as far posteriorly as the premolars, but not to the molars, which was likely the ancestral character state within our sample. It is worth noting that in all taxa examined in this study, the position of the cleft is largely anterior to the major chewing surfaces (molar teeth). Shallower clefts and deeper clefts appear to be derived conditions within Vespertilionidae, and no species in our sample exhibits closure of the cleft or posterior expansion past the first molar. In addition, among groups that evolved the shallowest and deepest clefts, there were no reversals to the ancestral, intermediate morphology. It is possible that there are biomechanical constraints on how far posteriorly a cleft can expand without compromising skull function during feeding, or the function of structures such as the nasal chamber. In addition, the correlation between relative width and relative length of the cleft, respectively, and cranial shape could indicate developmental constraints. For example, it is possible that cleft dimensions are limited by the development of adjacent bones, thus tracking changes in rostrum length and width during development. Exploring the limits of cleft dimensions and their relationship with cranial morphology and developmental patterns, especially in relation to sensory and respiratory structures, could shed light on possible biomechanical or developmental constraints on cleft morphology in bats.

Results from FE analyses showed support for our hypothesis that orofacial clefts reduce skull performance during biting in *L. cinereus*. Specifically, the cranium with a natural cleft was less efficient at transferring muscle force into bite force, and showed higher stress and strain, and lower safety factors when compared with the cranium with an artificially filled cleft. This suggests that the presence of a cleft reduces resistance to failure under load. Although we simplified the natural skull morphology to construct FE models for this study, differences in performance between the two models should be solely due to differences in cleft morphology. Therefore, it is likely that our results, at the very least, can illustrate the impact of a cleft on bite performance. Detailed data on the diet and physical properties of prey items consumed by this species, which are currently limited, would help corroborate this idea. Surprisingly, we observed similar regions of higher stress in the rostrum (dorsolateral surfaces and dorsomedial margin of the external narial aperture) and palate (posterolateral region and alveolar borders of the molars) between canine and molar bites in the model with a natural cleft. These similar concentrations of stress suggest that presence of a cleft can negatively impact skull performance while biting with teeth positioned posterior to the cleft border. This could, in turn, constrain how extreme cleft dimensions can become, as suggested by our geometric morphometrics results. It is worth noting, however, that maximum stress values estimated from all of our models were considerably lower than the level at which bone fails (140 MPa; Nordin and Frankel, 2001; Dumont et al., 2005), which indicates that, even with a large cleft, the skull of *L. cinereus* is well capable of withstanding most loads it could feasibly encounter during prey capture and feeding. In addition, the areas experiencing the highest stress across the entire cranium, and consequentially the regions most likely to fail at high stresses, were the zygomatic arches, and the sphenoid and palatine bones, as evidenced by the red and white regions on the crania in Figs 5 and 6.

Although our results suggest that presence of a midline cleft reduces some aspects of cranial performance during feeding (mechanical advantage, stress and strain), the mechanism(s) by which this trait has repeatedly evolved in bats remains elusive. Reduction of the premaxillary bone is a synapomorphy of Chiroptera (Giannini and Simmons, 2007; Hutcheon and Kirsch, 2006; Orr et al., 2016; Simmons and Geisler, 1998). Therefore, the morphospace within which the bat rostrum can evolve may be biased by conserved genetic and developmental factors, resulting in the repeated evolution of orofacial clefts as one of a limited set of possible morphologies (Alberch, 1989; Diogo, 2017; Felice et al., 2018; Galis, 1999). Additionally, the prevalence and repeated evolution of naturally occurring orofacial clefts in bats may indicate that this trait is adaptive for a function other than biting, or that their evolution is the consequence of a trade-off with another function that increases overall fitness. However, most of the functional hypotheses posed to explain the evolution of orofacial clefts in bats have yet to be tested, and there may be multiple mechanisms leading to the evolution of clefts in bats, as they show remarkable morphological diversity (Giannini and Simmons, 2007; Hutcheon and Kirsch, 2006; Orr et al., 2016; Simmons and Geisler, 1998). For instance, the presence of a flexible fibrous connective tissue in taxa with midline clefts likely increases the range of motion at the tip of the rostrum, which could facilitate increased gape for capture of larger prey items or production of a broader echolocation call beam (Kounitsky et al., 2015), or could improve dexterity for manipulating prey or grooming (Giannini and Simmons, 2007; Hutcheon and Kirsch, 2006; Orr et al., 2016; Simmons and Geisler, 1998). However, the degree to which rostral mobility is increased by the presence of a cleft, and how this impacts sensory functions, has not been investigated. Furthermore, replacement of bone with softer tissues could change how sound is transmitted through the snout as calls are emitted, or could also reduce skull mass for more efficient flight (Giannini and Simmons, 2007; Hutcheon and Kirsch, 2006; Orr et al., 2016; Simmons and Geisler, 1998).

Digital modeling methods allowed us to modify cleft morphology in a single skull; this in turn allowed us to test how the presence of a cleft impacts biting performance without introducing potentially confounding shape differences that would be encountered when comparing skull performance among different species. However,

future work comparing species from groups that independently evolved clefts, and represent a broader range of cleft morphologies, could greatly advance our understanding of why a trait that is detrimental in other mammals, and seems to impact biting and chewing performance in bats, is so common across this clade. In addition, building a better understanding of orofacial cleft morphological evolution, development and function in bats could shed light on maladaptive cleft palates in other taxa.

Acknowledgements
The authors are grateful to J. Davis, Z. J. Tseng and D. Pulaski for help with finite element methods and troubleshooting, and to P. Freeman for sharing data on jaw adductor masses. The authors also thank B. Patterson from the Field Museum of Natural History, E. Westwig, A. Marcato, E. Hoeger and B. O'Toole at the American Museum of Natural History, and J. Bradley at the Burke Museum for help with access to specimens.

Competing interests
The authors declare no competing or financial interests.

Author contributions
Conceptualization: A.A.C., J.H.A., S.E.S.; Methodology: A.A.C., J.H.A., S.E.S.; Formal analysis: A.A.C., J.H.A.; Investigation: A.A.C., J.H.A.; Resources: A.A.C., J.H.A., S.E.S.; Data curation: A.A.C., J.H.A.; Writing - original draft: A.A.C., J.H.A.; Writing - review & editing: A.A.C., J.H.A., S.E.S.; Visualization: A.A.C., J.H.A.; Supervision: A.A.C., S.E.S.; Project administration: A.A.C.; Funding acquisition: A.A.C., J.H.A., S.E.S.

Funding
This work was supported by National Science Foundation grant 1557125 to S.E.S., a Natural Sciences and Engineering Research Council of Canada Postdoctoral Fellowship to J.H.A, and a Gerstner Scholar Postdoctoral Fellowship at the American Museum of Natural History funded by the Gerstner Family Foundation to A.A.C.

Data availability
Finite element models are available from MorphoSource (Project P912) and morphometric data are available from the Dryad Digital Repository (Curtis et al., 2019): dryad.kwh70rz0k.

Supplementary information
Supplementary information available online at
http://jeb.biologists.org/lookup/doi/10.1242/jeb.196535.supplemental

References
Adams, D. C. (2014). A generalized *K* statistic for estimating phylogenetic signal from shape and other high-dimensional multivariate data. *Syst. Biol.* **63**, 685-697. doi:10.1093/sysbio/syu030

Adams, D. C. and Felice, R. N. (2014). Assessing trait covariation and morphological integration on phylogenies using evolutionary covariance matrices. *PLoS ONE* **9**, e94335. doi:10.1371/journal.pone.0094335

Adams, D. C. and Otárola-Castillo, E. (2013). Geomorph: an r package for the collection and analysis of geometric morphometric shape data. *Methods Ecol. Evol.* **4**, 393-399. doi:10.1111/2041-210X.12035

Alberch, P. (1989). The logic of monsters: evidence for internal constraint in development and evolution. *Geobios* **22**, 21-57. doi:10.1016/S0016-6995(89)80006-3

Arbour, J. H. and Brown, C. M. (2014). Incomplete specimens in geometric morphometric analyses. *Methods Ecol. Evol.* **5**, 16-26. doi:10.1111/2041-210X.12128

Blomberg, S. P., Garland, T. and Ives, A. R. (2003). Testing for phylogenetic signal in comparative data: behavioral traits are more labile. *Evolution* **57**, 717-745. doi:10.1111/j.0014-3820.2003.tb00285.x

Bohmann, K., Monadjem, A., Noer, C. L., Rasmussen, M., Zeale, M. R. K., Clare, E., Jones, G., Willerslev, E. and Gilbert, M. T. P. (2011). Molecular diet analysis of two African free-tailed bats (Molossidae) using high throughput sequencing. *PLoS ONE* **6**, e21441. doi:10.1371/journal.pone.0021441

Bollback, J. P. (2006). SIMMAP: Stochastic character mapping of discrete traits on phylogenies. *BMC Bioinformatics* **7**, 1-7. doi:10.1186/1471-2105-7-88

Brown, C. M., Arbour, J. H. and Jackson, D. A. (2012). Testing of the effect of missing data estimation and distribution in morphometric multivariate data analyses. *Syst. Biol.* **61**, 941-954. doi:10.1093/sysbio/sys047

Curtis, A. A., Arbour, J. H. and Santana, S. E. (2019). Mind the gap: natural cleft palates reduce biting performance in bats. *Dryad Digital Repository*. doi:10.5061/dryad.kwh70rz0k

Davis, J. L., Santana, S. E., Dumont, E. R. and Grosse, I. R. (2010). Predicting bite force in mammals: two-dimensional versus three-dimensional lever models. *J. Exp. Biol.* **213**, 1844-1851. doi:10.1242/jeb.041129

De Gueldre, G. and De Vree, F. (1988). Quantitative electromyography of the masticatory muscles of *Pteropus giganteus* (Megachiroptera). *J. Morphol.* **196**, 73-106. doi:10.1002/jmor.1051960107

Diogo, R. (2017). Etho-eco-morphological mismatches, an overlooked phenomenon in ecology, evolution and evo-devo that supports ONCE (organic nonoptimal constrained evolution) and the key evolutionary role of organismal behavior. *Front. Ecol. Evol.* **5**, 1-20. doi:10.3389/fevo.2017.00003

Diogo, R., Smith, C. M. and Ziermann, J. M. (2015). Evolutionary developmental pathology and anthropology: a new field linking development, comparative anatomy, human evolution, morphological variations and defects, and medicine. *Dev. Dyn.* **244**, 1357-1374. doi:10.1002/dvdy.24336

Diogo, R., Guinard, G. and Diaz, R. E., Jr. (2017). Dinosaurs, chameleons, humans, and evo-devo path: linking Étienne Geoffroy's teratology, Waddington's homeorhesis, Alberch's logic of "monsters," and Goldschmidt hopeful "monsters". *J. Exp. Zool.* **328**, 207-229. doi:10.1002/jez.b.22709

Dixon, M. J., Marazita, M. L., Beaty, T. H. and Murray, J. C. (2011). Cleft lip and palate: understanding genetic and environmental influences. *Nat. Rev. Genet.* **12**, 167-178. doi:10.1038/nrg2933

Dumont, E. R., Piccirillo, J. and Grosse, I. R. (2005). Finite-element analysis of biting behavior and bone stress in the facial skeletons of bats. *Anat. Rec.* **283A**, 319-330. doi:10.1002/ar.a.20165

Dumont, E. R., Grosse, I. R. and Slater, G. J. (2009). Requirements for comparing the performance of finite element models of biological structures. *J. Theor. Biol.* **256**, 96-103. doi:10.1016/j.jtbi.2008.08.017

Dumont, E. R., Dávalos, L. M., Goldberg, A., Santana, S. E., Rex, K. and Voigt, C. C. (2012). Morphological innovation, diversification and invasion of a new adaptive zone. *Proc. R. Soc. B Biol. Sci.* **279**, 1797-1805. doi:10.1098/rspb.2011.2005

Erickson, G. M., Cantanese, J. and Keaveny, T. M. (2002). Evolution of the biomechanical properties of the femur. *Anat. Rec.* **268**, 115-124. doi:10.1002/ar.10145

Erwin, D. H. (2015). Novelty and innovation in the history of life. *Curr. Biol.* **25**, R930-R940. doi:10.1016/j.cub.2015.08.019

Felice, R. N., Randau, M. and Goswami, A. (2018). A fly in a tube: macroevolutionary expectations for integrated phenotypes. *Evolution* **72**, 1-15. doi:10.1111/evo.13608

Freeman, P. W. (1979). Specialized insectivory: beetle-eating and moth-eating molossid bats. *J. Mammal.* **60**, 467-479. doi:10.2307/1380088

Freeman, P. W. (1981). Correspondence of food habits and morphology in insectivorous bats. *J. Mammal.* **62**, 166-173. doi:10.2307/1380489

Freeman, P. W. (1992). Canine teeth of bats (Microchiroptera): size, shape and role in crack propagation. *Biol. J. Linn. Soc.* **45**, 97-115. doi:10.1111/j.1095-8312.1992.tb00634.x

Freeman, P. W. (1998). Form, function, and evolution in skulls and teeth of bats. In *Bat Biology and Conservation* (ed. T. H. Kunz and P. A. Racey), pp. 140-156. Washington, DC: Smithsonian Institution Press.

Freeman, P. W. and Lemen, C. A. (2007). Using scissors to quantify hardness of insects: Do bats select for size or hardness? *J. Zool.* **271**, 469-476. doi:10.1111/j.1469-7998.2006.00231.x

Freeman, P. W. and Lemen, C. A. (2010). Simple predictors of bite force in bats: the good, the better and the better still. *J. Zool.* **282**, 284-290. doi:10.1111/j.1469-7998.2010.00741.x

Galis, F. (1999). Why do almost all mammals have seven cervical vertebrae? Developmental constraints, Hox genes, and cancer. *J. Exp. Zool.* **285**, 19-26. doi:10.1002/(SICI)1097-010X(19990415)285:1<19::AID-JEZ3>3.0.CO;2-Z

Giannini, N. P. and Simmons, N. B. (2007). The chiropteran premaxilla: a reanalysis of morphological variation and its phylogenetic interpretation. *Am. Museum Novit.* **3585**, 1-44. doi:10.1206/0003-0082(2007)3585[1:TCPARO]2.0.CO;2

Gilbert, M. M., Snively, E. and Cotton, J. (2016). The tarsometatarsus of the ostrich *Struthio camelus*: anatomy, bone densities, and structural mechanics. *PLoS ONE* **11**, e0149708. doi:10.1371/journal.pone.0149708

Grosse, I. R., Dumont, E. R., Coletta, C. and Tolleson, A. (2007). Techniques for modeling muscle-induced forces in finite element models of skeletal structures. *Anat. Rec.* **290**, 1069-1088. doi:10.1002/ar.20568

Gunz, P., Mitteroecker, P., Neubauer, S., Weber, G. W. and Bookstein, F. L. (2009). Principles for the virtual reconstruction of hominin crania. *J. Hum. Evol.* **57**, 48-62. doi:10.1016/j.jhevol.2009.04.004

Herrel, A., De Smet, A., Aguirre, L. F. and Aerts, P. (2008). Morphological and mechanical determinants of bite force in bats: do muscles matter? *J. Exp. Biol.* **211**, 86-91. doi:10.1242/jeb.012211

Horn, J. L. (1965). A rationale and test for the number of factors in factor analysis. *Psychometrika* **30**, 179-185. doi:10.1007/BF02289447

Huelsenbeck, J. P., Nielsen, R. and Bollback, J. P. (2003). Stochastic mapping of morphological characters. *Syst. Biol.* **52**, 131-158. doi:10.1080/10635150390192780

Hutcheon, J. M. and Kirsch, J. A. W. (2006). A moveable face: deconstructing the Microchiroptera and a new classification of extant bats. *Acta Chiropt.* **8**, 1-10. doi:10.3161/1733-5329(2006)8[1:AMFDTM]2.0.CO;2

Hylander, W. L., Ravosa, M. J. and Ross, C. (2004). Jaw muscle recruitment patterns during mastication in anthropoids and prosiminans. In *Shaping Primate Evolution* (ed. F. Anapol, R. Z. German and N. G. Jablonski), pp. 229-257. Cambridge: Cambridge University Press.

Kounitsky, P., Rydell, J., Amichai, E., Boonman, A., Eitan, O., Weiss, A. J. and Yovel, Y. (2015). Bats adjust their mouth gape to zoom their biosonar field of view. *Proc. Natl. Acad. Sci. USA* **112**, 6724-6729. doi:10.1073/pnas.1422843112

Krief, S., Watts, D. P., Mitani, J. C., Krief, J.-M., Cibot, M., Bortolamiol, S., Seguya, A. G. and Couly, G. (2015). Two cases of cleft lip and other congenital anomalies in wild chimpanzees living in Kibale National Park, Uganda. *Cleft Palate-Craniofacial J.* **52**, 743-750. doi:10.1597/14-188

Myers, P., Lundrigan, B. L., Gillespie, B. W. and Zelditch, M. L. (1996). Phenotypic plasticity in skull and dental morphology in the prairie deer mouse (*Peromyscus maniculatus bairdii*). *J. Morphol.* **229**, 229-237. doi:10.1002/(SICI)1097-4687(199608)229:2<229::AID-JMOR7>3.0.CO;2-W

Nordin, M. and Frankel, V. H. (2001). *Basic Biomechanics of the Musculoskeletal System*, 3rd edn. Philadelphia: Lippincott Williams and Eilkins.

Oba, S., Sato, M.-A., Takemasa, I., Monden, M., Matsubara, K.-I. and Ishii, S. (2003). A Bayesian missing value estimation method for gene expression profile data. *Bioinformatics* **19**, 2088-2096. doi:10.1093/bioinformatics/btg287

Orr, D. J. A., Teeling, E. C., Puechmaille, S. J. and Finarelli, J. A. (2016). Patterns of orofacial clefting in the facial morphology of bats: a possible naturally occurring model of cleft palate. *J. Anat.* **229**, 657-672. doi:10.1111/joa.12510

Paradas-Lara, I., Casado-Gómez, I., Martín, C., Martínez-Sanz, E., López-Gordillo, Y., González, P., Rodríguez-Bobada, C., Chamorro, M., Arias, P., Maldonado, E. et al. (2014). Maxillary growth in a congenital cleft palate canine model for surgical research. *J. Cranio-Maxillofacial Surg.* **42**, 13-21. doi:10.1016/j.jcms.2013.01.032

Peres-Neto, P. R., Jackson, D. A. Somers, K. M. (2005). How many principal components? Stopping rules for determining the number of non-trivial axes revisited. *Comp. Stat. Data Anal.* **49**, 974-997. doi:10.1016/j.csda.2004.06.015

Revell, L. J. (2009). Size-correction and principal components for interspecific comparative studies. *Evolution* **63**, 3258-3268. doi:10.1111/j.1558-5646.2009.00804.x

Revell, L. J. (2012). phytools: an R package for phylogenetic comparative biology (and other things). *Methods Ecol. Evol.* **3**, 217-223. doi:10.1111/j.2041-210X.2011.00169.x

Rohlf, F. J. and Corti, M. (2000). Use of two-block partial least-squares to study covariation in shape. *Syst. Biol.* **49**, 740-753. doi:10.1080/106351500750049806

Santana, S. E. (2018). Comparative anatomy of bat jaw musculature via diffusible iodine-based contrast-enhanced computed tomography. *Anat. Rec.* **301**, 267-278. doi:10.1002/ar.23721

Santana, S. E. and Cheung, E. (2016). Go big or go fish: morphological specializations in carnivorous bats. *Proc. R. Soc. B* **283**, 20160615. doi:10.1098/rspb.2016.0615

Santana, S. E. and Dumont, E. R. (2011). Do roost-excavating bats have stronger skulls? *Biol. J. Linn. Soc.* **102**, 1-10. doi:10.1111/j.1095-8312.2010.01551.x

Santana, S. E., Dumont, E. R. and Davis, J. L. (2010). Mechanics of bite force production and its relationship to diet in bats. *Funct. Ecol.* **24**, 776-784. doi:10.1111/j.1365-2435.2010.01703.x

Santana, S. E., Grosse, I. R. and Dumont, E. R. (2012). Dietary hardness, loading behavior, and the evolution of skull form in bats. *Evolution.* **66**, 2587-2598. doi:10.1111/j.1558-5646.2012.01615.x

Satokata, I. and Maas, R. (1994). Msx1 deficient mice exhibit cleft palate and abnormalities of craniofacial and tooth development. *Nat. Genet.* **6**, 348-356. doi:10.1038/ng0494-348

Shi, J. J. and Rabosky, D. L. (2015). Speciation dynamics during the global radiation of extant bats. *Evolution* **69**, 1528-1545. doi:10.1111/evo.12681

Shi, J. J., Westeen, E. P. and Rabosky, D. L. (2018). Digitizing extant bat diversity: An open-access repository of 3D μCT-scanned skulls for research and education. *PLoS ONE* **13**, e0203022. doi:10.1371/journal.pone.0203022

Simmons, N. B. (2005). Order Chiroptera. In *Mammal Species of the World: A Taxonomic and Geographic Reference* (ed. D. E. Wilson and D. M. Reeder), pp. 312-529. Baltimore: Johns Hopkins University Press.

Simmons, N. B. and Geisler, J. H. (1998). Phylogenetic relationships of *Icaronycteris*, *Archaeonycteris*, *Hassianycteris*, and *Palaeochiropteryx* to extant bat lineages, with comments on the evolution of echolocation and foraging strategies in Microchiroptera. *Bull. Am. Museum Nat. Hist.* **235**, 4-182.

Slater, G. J., Dumont, E. R. and Van Valkenburgh, B. (2009). Implications of predatory specialization for cranial form and function in canids. *J. Zool.* **278**, 181-188. doi:10.1111/j.1469-7998.2009.00567.x

Tseng, Z. J. and Wang, X. (2011). Do convergent ecomorphs evolve through convergent morphological pathways? Cranial shape evolution in fossil hyaenids and borophagine canids (Carnivora, Mammalia). *Paleobiology* **37**, 470-489. doi:10.1666/10007.1

Wroe, S., McHenry, C. and Thomason, J. (2005). Bite club: comparative bite force in big biting mammals and the prediction of predatory behaviour in fossil taxa. *Proc. R. Soc. B* **272**, 619-625. doi:10.1098/rspb.2004.2986